Materials & Design 250 (2025) 113576

Contents lists available at ScienceDirect

Materials & Design

journal homepage: www.elsevier.com/locate/matdes

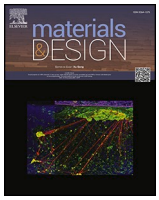

Atomistic behavior of Cu–Cu solid-state bonding in polycrystalline Cu with high-density boundaries

Hiroaki Tatsumi [a,*], C.R. Kao [b], Hiroshi Nishikawa [a]

[a] Joining and Welding Research Institute, Osaka University, 11-1 Mihogaoka, Ibaraki, Osaka 567-0047, Japan
[b] Department of Materials Science and Engineering, National Taiwan University, No. 1, Sec. 4, Roosevelt Road, Taipei 10617, Taiwan

ARTICLE INFO

Keywords:
Atomistic modeling
Cu–Cu solid-state bonding
Grain boundaries (GBs)
Molecular dynamics simulations
Nanocrystalline (NC) structure

ABSTRACT

Low-temperature Cu–Cu solid-state bonding is key for interconnect miniaturization and higher current densities in advanced semiconductor devices. Achieving reliable joints requires effective void closure at the interface, driven by diffusion. We employed molecular dynamics simulations to elucidate the dominant atomic transport mechanism enhancing void closure. We modeled two polycrystalline Cu structures with high-density boundaries—a randomly oriented nanocrystalline (NC) structure with high-density grain boundaries (GBs) and a unidirectional [111]-oriented columnar nanotwinned (NT) structure with high-density twin boundaries (TBs). Thermocompression bonding was simulated for both structures, with the bonding surfaces designed to replicate surface roughness. The NC structure exhibited significant atomic movement at the GBs with simultaneous grain coalescence, leading to early void closure. In contrast, the NT structure showed limited atomic movement and void closure, despite active surface diffusion. Potential energy analysis revealed that the NC structure's energy decreased significantly over time, promoting void closure, while the NT structure's quasi-stable energy state hindered this process. This was attributed to its high potential energy state, low activation energy for GB diffusion, and complex GB migration during grain coalescence at randomly oriented GBs. This study provides a deeper understanding of the GB-driven atomic transport mechanism that promotes void closure.

1. Introduction

The rapid development of advanced electronic devices featuring higher integrated levels and increased electrical current density has heightened the demand for advanced bonding solutions. Traditional Sn-based solder joints, commonly employed in electronic device assembly, are approaching their performance limits. This challenge is particularly pronounced in cutting-edge three-dimensional integrated circuits (3D-ICs), where the input/output pitch is expected to decrease to less than 1 μm [1]. Reducing the size of solder bumps can lead to degraded joint characteristics due to the formation of Kirkendall voids and brittle intermetallic compounds at the interface [2–4]. Additionally, solder joints deteriorate with increasing current density and temperature gradients, owing to electromigration and thermomigration processes [5,6].

To address these challenges, Cu–Cu solid-state bonding has garnered significant attention as a promising assembly technology [7–10]. To achieve successful Cu–Cu bonding, normal coarse-grained Cu typically requires a bonding temperature above 300 °C, which exceeds the preferred bonding temperature for advanced interconnections [11,12]. After successfully removing oxides and impurities from the bonding surfaces, void closure at the bonding interface must be ensured [13]. Diffusion phenomena play a pivotal role in enabling bonding under low-temperature conditions, which are highly desirable for semiconductor applications. One potential dominant diffusion mechanism facilitating the Cu–Cu bonding is surface diffusion. Highly [111]-oriented columnar-grained Cu with high-density twin boundaries (TBs), known as nanotwinned (NT) Cu, has been proposed to enhance bondability. This is based on the fact that the surface diffusion coefficient of Cu on the (111) plane is three to four orders of magnitude higher than that on the other surfaces [14,15]. Another plausible mechanism is grain boundary (GB) diffusion. Nanocrystalline (NC) Cu, formed through physical vapor deposition [16] or electrochemical deposition [17,18], has demonstrated the ability to bond at lower temperature than coarse-grained Cu, implying that the significant GB diffusion enhances bondability. Nevertheless, a more detailed understanding of how different diffusion pathways, characterized by grain structures, affect bonding behavior is essential to promote diffusion adjacent to the bonding interface and to achieve low-temperature bonding.

* Corresponding author at: Joining and Welding Research Institute, Osaka University, 11-1 Mihogaoka, Ibaraki, Osaka 567-0047, Japan.
E-mail addresses: tatsumi.jwri@osaka-u.ac.jp (H. Tatsumi), crkao@ntu.edu.tw (C.R. Kao), nisikawa.jwri@osaka-u.ac.jp (H. Nishikawa).

https://doi.org/10.1016/j.matdes.2024.113576
Received 14 September 2024; Received in revised form 6 December 2024; Accepted 26 December 2024
Available online 30 December 2024

Molecular dynamics (MD) simulation, a technique for atomistic-scale modeling, is a powerful tool for evaluating bonding behavior and diffusion phenomena. Using MD simulations, the diffusion phenomena at the Al–Cu [19] and Cu–Cu [20,21] solid-state diffusion-bonded interfaces have been extensively investigated. Furthermore, in our previous study [22], we investigated the impact of crystalline orientation on Cu–Cu bonding behavior using monocrystalline Cu models, focusing on void closure at the bonding interface, atomic displacement magnitude, and the related diffusion coefficients. These studies reveal that MD simulations should provide insight into the diffusion behavior driven by boundaries— surfaces, GBs, or TBs—at the Cu–Cu bonding interface.

In this study, we employed MD simulations to investigate atomic movement and void-closure mechanisms at the bonding interfaces of Cu–Cu joints with different grain structures. To enhance atomic movement during bonding, we modeled two polycrystalline Cu structures with high-density boundaries, namely a randomly oriented NC structure and a unidirectional [111]-oriented columnar NT structure. We subjected polycrystalline Cu models, which included bonding interfaces that simulated surface roughness, to thermocompression bonding. Subsequently, we examined the void-closure behavior at the interface, grain structure evolution, atomic displacement, and changes in potential energy during bonding. Based on these observations, herein we discuss the role of high-density boundaries in influencing void-closure behavior.

2. Simulation methodology

NC and NT slabs were prepared for MD simulations, with the models

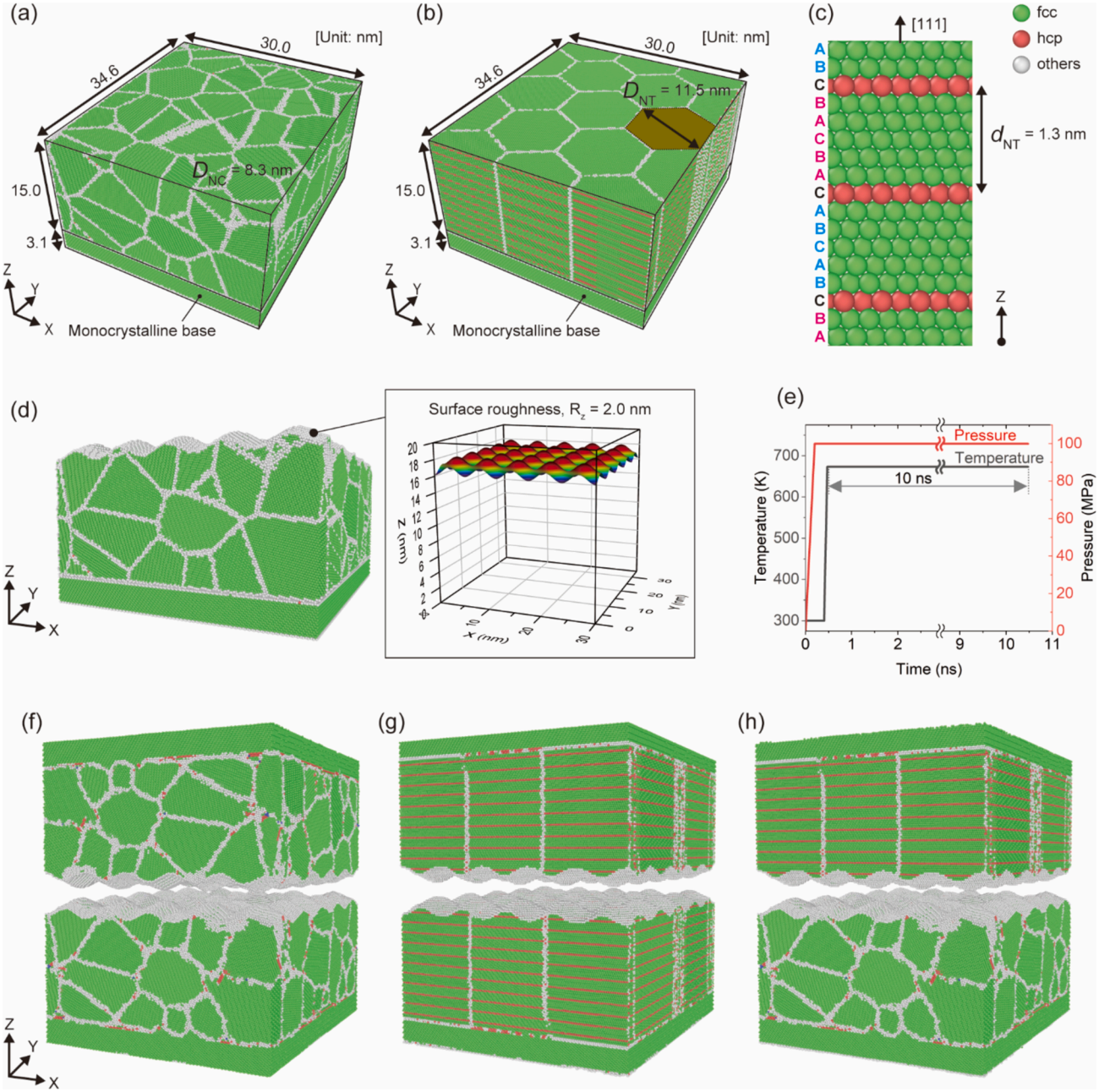

Fig. 1. MD simulation setup of polycrystalline Cu–Cu joint models illustrating configurations and conditions. (a) Nanocrystalline (NC) slab with an average grain size (D_{NC}) of 8.3 nm. (b) Nanotwinned (NT) slab with a grain size (D_{NT}) of 11.5 nm. (c) Cross-sectional view of twin boundary (TB) atom arrangement in (b). (d) Surface roughness (R_z = 2.0 nm), with inset showing the surface profile. (e) Temperature and pressure profiles during the simulation. (f) NC-NC, (g) NT-NT, and (h) NC-NT joints.

and procedures displayed in Fig. 1. Atoms were color coded based on their structures: green for face centered cubic (FCC), red for hexagonal close-packed (HCP), and white for other structures. The NC slab (Fig. 1 (a)) was designed to be periodic in the X and Y directions, with dimensions of 30.0 and 34.6 nm, respectively. In the Z direction, a 15.0 nm thick NC layer was placed on a monocrystalline base layer that was 3.1 nm thick and < 111 > oriented along the Z axis. The base layer was included to prevent divergence due to model collapse during the calculations. The NC layer was divided into multiple randomly oriented grains using Voronoi tessellation, with 50 randomly placed nodes in a given space. The average grain size of the NC layer, D_{NC}, was set at 8.3 nm.

The NT slab was designed to have the same periodicity and dimensions in the X and Y directions as those of the NC slabs (Fig. 1(b)). Similarly, in the Z direction, the NT layer was placed on top of the monocrystalline base layer. The NT layer was modeled with hexagonal columnar grains arranged in the X–Y plane, oriented in the < 111 > direction along the Z axis, with a random rotation angle around the < 111 > axis for each grain. This structure was inspired by a previously reported electrodeposited NT layer [23], which consisted of unidirectional columnar grains. The grain size, D_{NT}, expressed as the width of the hexagon, was set at 11.5 nm. The hexagonal columnar grains contained TBs (red atoms, Fig. 1(c)). They were constructed through continuous atomic displacements on the adjacent (111) planes, creating symmetric twins while preserving the matrix structure [24]. The spacing between the twin boundaries, d_{NT}, was set at 1.3 nm.

To simulate the surface roughness of the bonding surface, a two-dimensional sinusoidal surface with periodic geometry was applied to both the NC and NT slabs (Fig. 1(d)). This surface was characterized by a periodic array of 5 × 5 peaks, with a height difference between the peaks and valleys (surface roughness, R_Z) of 2 nm. These simulation models were prepared using the atomic-scale modeling software ATOMSK [25].

MD simulations were conducted using Large-scale Atomic/Molecular Massively Parallel Simulator (LAMMPS) software [26]. The initial atomic velocities were randomly assigned a Gaussian distribution based on the set temperature. Newton's equations of motion were integrated using the Verlet algorithm with a fixed timestep of 1 fs. The atomic interactions were described using the embedded atomic method (EAM) potential for Cu developed by Mishin et al. [27], which accurately models various material properties including stacking fault energy. Each slab was equilibrated at 300 K for 200 ps. Subsequently, the relaxed NC and NT slabs were combined to form NC-NC, NT-NT, and NC-NT joint models (Fig. 1(f–h), respectively), containing approximately 3 000 000 atoms. After further equilibration at 300 K for 400 ps, the joint models were heated from 300 K to a bonding temperature of 673 K at a heating rate of 5×10^{12} K/s, while maintaining a bonding pressure of 100 MPa, and held at this temperature for 10 ns (Fig. 1(e)). Details of this procedure can be found in our previous study [22]. Additionally, the potential energies of each atom were calculated using MD simulations.

The simulated configurations were investigated using the open visualization tool software OVITO [28]. Polyhedral template matching (PTM) [29], which identifies local crystalline structures, was employed for visualization. The PTM approach categorizes atoms into three types: green for FCC, red for HCP (corresponding to stacking faults and TBs), and white for disordered atoms (corresponding to GB and surface atoms). Surface atoms were identified using the alpha-shaped algorithm [30]. The void-closure behavior at the bonding interface was then evaluated by measuring the relative density change at the bonding interface. A 4 nm thick region, including the surface roughness, was defined as the initial volume of the bonding interface, and the volume change in this region during the simulation period was recorded. Additionally, atomic displacements were quantitatively assessed in terms of the mean square displacement (MSD) along the X, Y, or Z directions. The aforementioned analysis methods are detailed in [22].

3. Results

3.1. Void closure at the bonding interface and grain structure evolution

The void-closure behavior was quantitatively investigated by analyzing the relative density change at the bonding interface (Fig. 2 (a)). The relative density increased over time for both the NC-NC and NC-NT joints (Fig. 2(b)), indicating early void closure. This increase was more pronounced for the NC-NC joint than for the NC-NT joint. In contrast, the NT-NT joint displayed little change in relative density over time, suggesting that significant void closure did not occur within the simulation timeframe. These results suggest that the NC slab contributed to early void closure.

The evolution of the grain structures in NC-NC, NT-NT, and NC-NT joints at 673 K over timesteps of 0, 0.5, 2.0, 5.0, and 10 ns is illustrated in Fig. 3. At a time step of 0 ns, elliptical voids were observed at the joint interface for all joint types. In the NC-NC joint (Fig. 3(a) and video S1), interfacial void closure and grain coarsening were observed over time. Some voids were already closed by 0.5 ns, and all voids in this cross-section were closed by 2.0 ns. Grain coarsening occurred simultaneously with a reduction in the GB regions, as represented by white atoms. Red atoms, indicating local twinning deformation, were also observed. In contrast, the NT-NT joint (Fig. 3(b) and video S2) did not display any void closure at the bonding interface within the simulation timeframe, which is consistent with the relative density changes shown in Fig. 2(b). Regarding the grain structure, longitudinal GBs and horizontal TBs were initially observed. Over time, while the GBs decreased, the TBs remained consistent, indicating that the TBs were more stable than the GBs. The NC-NT joint (Fig. 3(c) and video S3) exhibited intermediate behavior between those observed in the NC-NC and NT-NT joints. Specifically, the voids initially present at the bonding interface gradually closed, albeit slower than those in the NC-NC bonding. Regarding the grain structure, grains on the NC slab side coarsened and the GBs decreased over time, while on the NT slab side, the GBs also decreased but the TBs remained largely unchanged.

To quantitatively understand the grain structure evolutions, the proportions of TB, GB, and surface atoms in the NC-NC, NT-NT, and NC-NT joints were evaluated; the monocrystalline base layer was excluded from the analysis (Fig. 4). The sum of the proportions of TB, GB, surface, and intrinsic atoms is equal to one, and the proportion of intrinsic atoms is not shown in this figure. At 0 ns, the total proportion of atoms in the TB, GB, and surface regions was approximately 24 % for all types of joints, with the ratio of surface atoms remaining constant at 2.5 %. In the NC-NC joint (Fig. 4(a)), the proportion of GB atoms decreased from 20 % to 11 %, that of TB atoms slightly increased from 1.3 % to 3.7 %, and that of surface atoms decreased from 2.5 % to 0.8 %. These changes indicate grain coarsening, the introduction of stacking faults, and void closure at the bonding interface. In contrast, in the NT-NT joint (Fig. 4(b)), the TB atoms remained stable at approximately 13 %, the GB atoms decreased from 8.4 % to 4.5 %, and the surface atoms remained stable at 2.5 %. This indicates grain coarsening but with no significant changes in the TBs or void regions. The NC-NT joint (Fig. 4(c)) exhibited an intermediate behavior between those of the NC-NC and NT-NT joints. The proportions of the GB, TB, and surface atoms reflect the characteristics of both the NC and NT structures, indicating moderate grain coarsening and some void closure at the bonding interface.

In summary, NC structures with abundant GBs exhibited early void closure at the bonding interface, which was facilitated by significant atomic rearrangement during grain coarsening. In contrast, NT structures with numerous TBs scarcely promoted void closure owing to the stability of the TBs, which provided minimal atomic rearrangement.

3.2. Atomic movement behavior at the bonding interface

To clarify the atomic movement behavior related to void closure and grain growth, atomic displacement vector analysis was performed

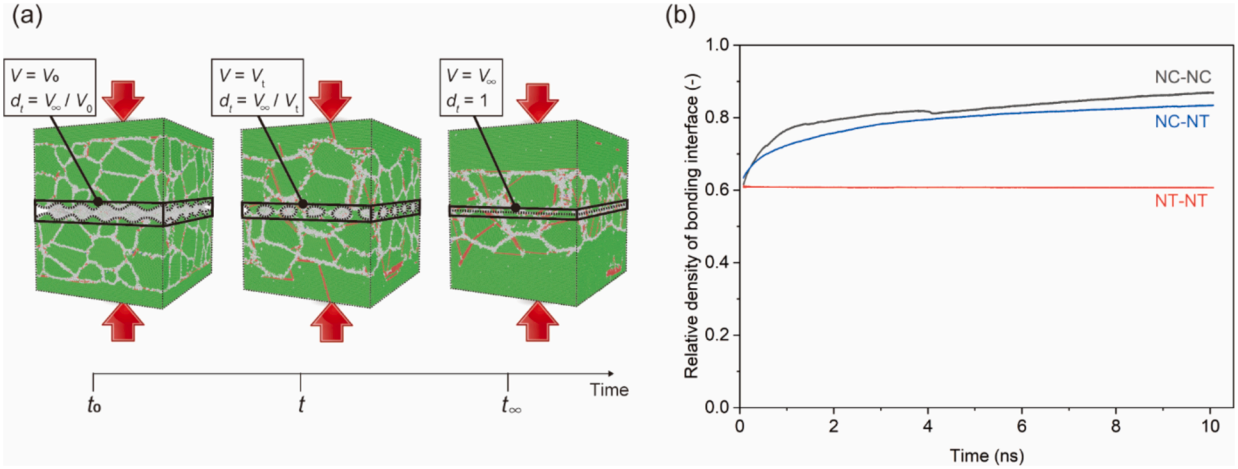

Fig. 2. Relative density evolution of the bonding interface in polycrystalline Cu–Cu joint models. (a) Schematic of relative density evolution of the bonding interface and (b) Relationship between simulation time and relative density of the bonding interface at 673 K.

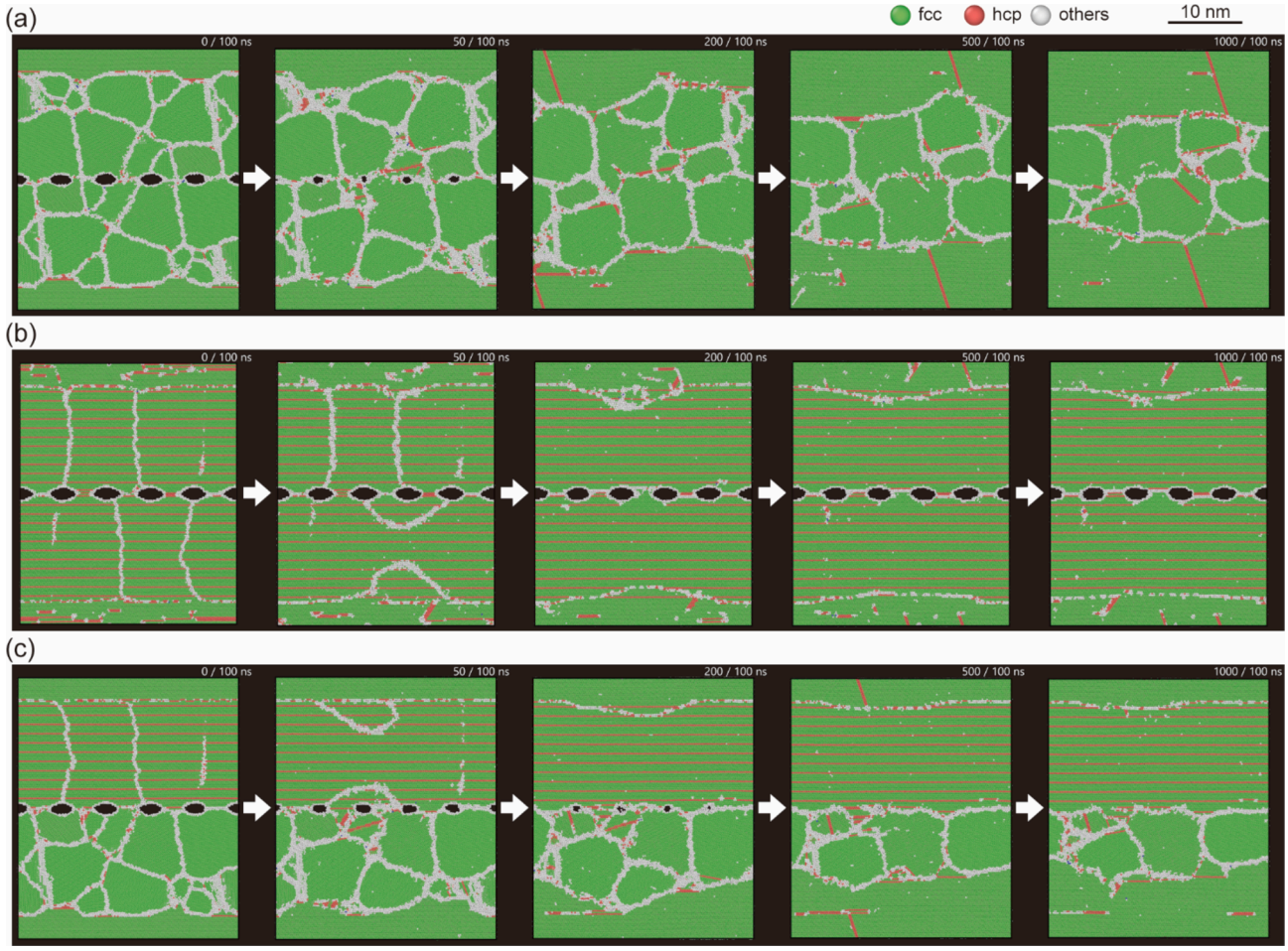

Fig. 3. Evolution of the grain structure at the bonding interface at 673 K over time steps of 0, 0.5, 2.0, 5.0, and 10 ns for (a) NC-NC, (b) NT-NT, and (c) NC-NT joints.

(Fig. 5). Fig. 5(a–c) illustrate the grain structures adjacent to the bonding interface at 0 and 10 ns in the three types of joints, magnified from Fig. 3. In the NC-NC joint (Fig. 5(d) and video S4), significant atomic movement toward the voids was observed at the GBs and bonding interface. In contrast, the NT-NT joint (Fig. 5(e) and video S5) exhibited significant movement only for atoms on the void surface, with minimal movement observed for the atoms at the GBs, TBs, and bonding interfaces. Within the grains, the displacement magnitude of atoms in the NC-NC joint was greater than that in the NT-NT joint, which was attributed to the atomic rearrangement associated with grain coarsening. The NC-NT joint (Fig. 5(f) and video S6) exhibited the characteristics of both the NC and NT structures. Atoms in the NC regions displayed significant movement, particularly at the GBs and bonding interface, which contributed to void closure. In contrast, in the NT

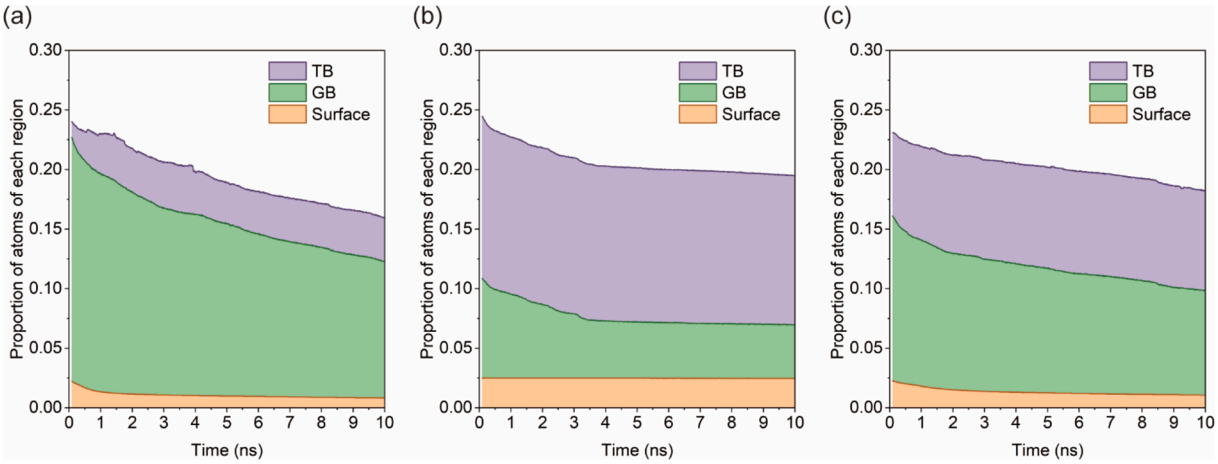

Fig. 4. Proportion of atoms in TB, GB, and surface regions in (a) NC-NC, (b) NT-NT, and (c) NC-NT joints; the proportion of intrinsic atoms is not shown in the figure.

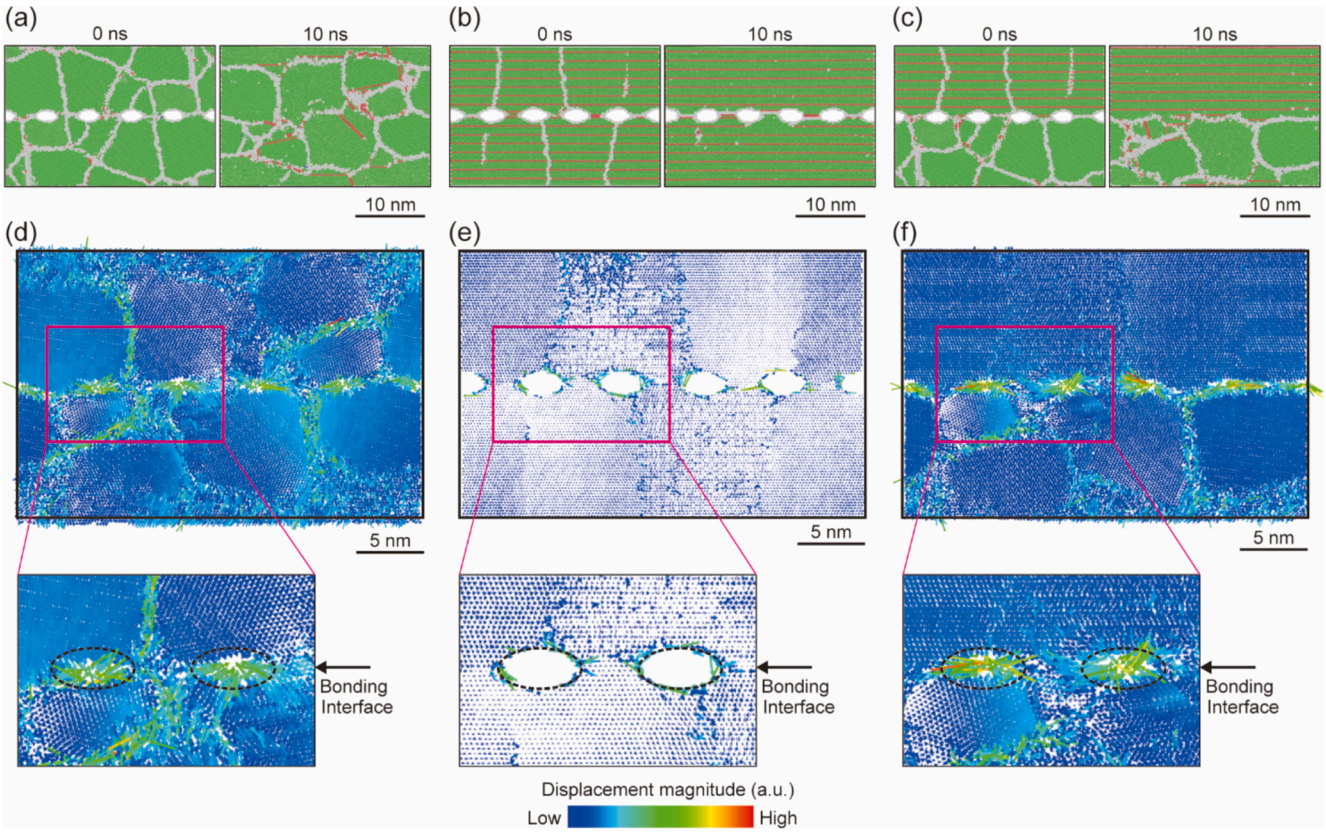

Fig. 5. Atomic displacement behavior at the bonding interface. Interfacial crystalline structure of (a) NC-NC, (b) NT-NT, and (c) NC-NT joints. Atomic displacement magnitude for (d) NC-NC, (e) NT-NT, and (f) NC-NT joints over a time step of 10 ns; initial gaps are presented by dotted lines.

regions, the atomic displacement was relatively small, reflecting the stability of the TBs. It is noteworthy that even the atomic movement in the NT region was activated by the combination with the NC region.

The MSDs were next calculated to quantitatively evaluate the magnitude and direction of atomic displacement along the X, Y, and Z directions (Fig. 6). The MSDs of the NC structures were significantly higher than those of the NT structures, confirming the higher atomic mobilities observed in Fig. 5. In the NC structures, the displacement was relatively uniform across all directions. Meanwhile, in the NT structures, the MSDs in the X and Y directions (in-plane) were larger than those in the Z direction (out-of-plane), indicating less atomic movement in the Z direction. Furthermore, when comparing the MSD of the NT structure in each joint, its MSD with the NC structure (Fig. 6(c)) was larger than that with the same type (Fig. 6(b)). This quantitatively supports the difference in atomic displacement seen in Fig. 5.

In summary, atomic displacement vector analysis revealed significant atomic movement at the GBs of randomly oriented grains within the NC structures, leading to void closure. In contrast, minimal atomic movement, particularly along the Z axis, was observed in the TBs and GBs within the unidirectional columnar grains of the NT structures. Consequently, although the movement of atoms on the void surface was significant, their contribution to void closure was limited. Furthermore, the NC structure activated the atomic movement of the NT structure. These findings highlight the critical role of atomic movement at random

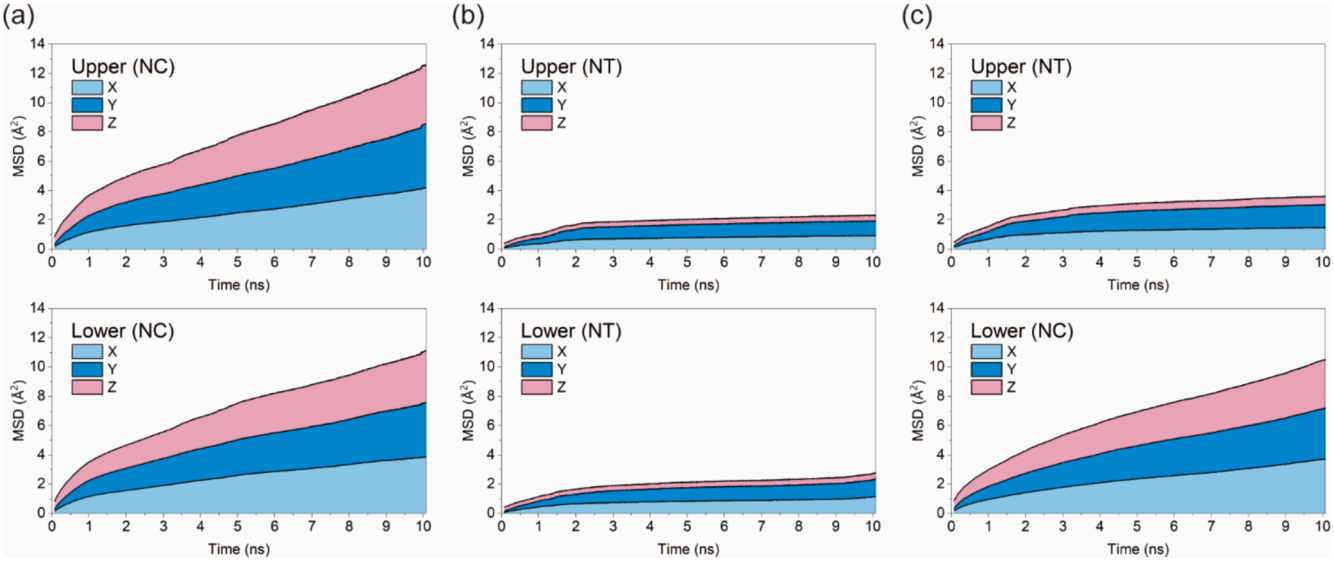

Fig. 6. Calculated MSDs for (a) NC-NC, (b) NT-NT, and (c) NC-NT joints along the X, Y, and Z directions; top and bottom figures represent the upper and lower slabs, respectively.

GBs in promoting void closure.

4. Discussion

This study investigated the atomic movement behavior and void-closure mechanisms at the bonding interfaces of Cu–Cu joints with different grain structures. The results demonstrated that the NC structures exhibited significant atomic movement at the GBs, leading to early void closure. In contrast, in the NT structures, while the atomic movement at the void surface was significant, the movement of other atoms was minimal, resulting in limited void closure. In Section 4, we provide an energy-based interpretation of the atomic movement behavior and void-closure mechanisms observed in each grain structure.

Figs. 7(a–c) illustrate the variation in potential energy over time for each joint, whereas Fig. 7(d–f) present the cross-sectional views of the potential energy distribution of atoms near the bonding interface. In the NC-NC joint (Fig. 7(a)), the potential energies in the upper and lower NC regions were initially high but significantly decreased over time. The corresponding potential energy distribution (Fig. 7(d)) showed that at 0 ns, the GB and surface atoms of the voids had high potential energy, whereas at 10 ns, the regions with high-energy GB and surface atoms were greatly reduced because of grain coarsening and void closure.

In the NT-NT joint (Fig. 7(b)), the potential energies in the upper and lower NT regions were low from the initial state, decreased slightly

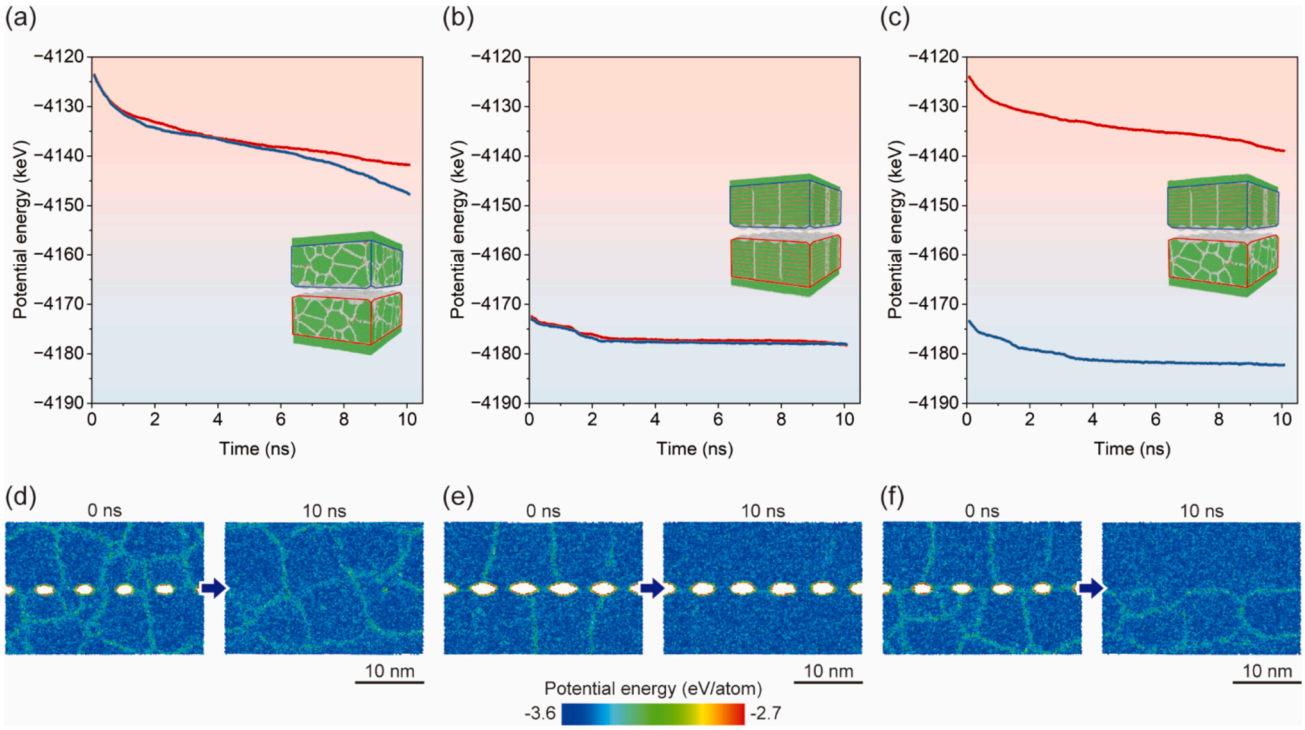

Fig. 7. Evolution of potential energy in (a) NC-NC, (b) NT-NT, and (c) NC-NT joints; red and blue lines represent the lower and upper slabs, respectively. Potential energy distributions within crystalline structures over time steps of 0 and 10 ns in (d) NC-NC, (e) NT-NT, and (f) NC-NT joints.

during the first 2 ns, and remained nearly constant thereafter. The corresponding potential energy distribution (Fig. 7(e)) revealed that at 0 ns, the GB and surface atoms of the voids exhibited high potential energies, whereas the TB atoms exhibited low potential energies, similar to those in the intrinsic region. After 10 ns, grain coarsening reduced the high-energy GB region; however, the surface atoms maintained high potential energy. The NC-NT joint (Fig. 7(c)) exhibited intermediate behavior, combining the trends of both the NC and NT structures. Similar to earlier observations, the GB and void surface atoms initially exhibited high potential energies; however, after 10 ns, only the GB atoms in the NC region exhibited high energies (Fig. 7(f)). It should be noted that the potential energy of NT region was slightly reduced by combining with the NC region (compare Fig. 7(b) and (c)).

The average potential energies per atom in each region were next evaluated (Fig. 8). The results indicated that these values remained constant over time, which is inherent to local crystalline structures. The average potential energies per atom of the local crystalline structures, obtained in the last 5 ns are listed in Table 1. The intrinsic region exhibited the lowest potential energy per atom, followed closely by the TB region. The GB region exhibited higher energies, and the surface region displayed the highest values. These results indicated that the intrinsic and TB atoms were stable, whereas the surface and GB atoms were unstable.

The potential energy change of the entire system with N number of atoms is determined by the evolution of the local crystal structures and the corresponding potential energies of their atoms. This can be expressed using the equation

$$\Delta E^N = E_{\text{intrinsic}} \bullet \Delta N_{\text{intrinsic}} + E_{\text{TB}} \bullet \Delta N_{\text{TB}} + E_{\text{GB}} \bullet \Delta N_{\text{GB}} + E_{\text{surf.}} \bullet \Delta N_{\text{surf.}} \quad (1)$$

where, ΔE^N represents the potential energy change of the entire system with N number of atoms. $E_{\text{intrinsic}}$, E_{TB}, E_{GB}, and $E_{\text{surf.}}$, and $\Delta N_{\text{intrinsic}}$, ΔN_{TB}, ΔN_{GB}, and $\Delta N_{\text{surf.}}$ denote the average potential energies per atom and the changes in the number of atoms in the intrinsic, TB, GB, and surface regions, respectively. The total change in the number of atoms across all regions must be zero:

$$\Delta N_{\text{intrinsic}} + \Delta N_{\text{TB}} + \Delta N_{\text{GB}} + \Delta N_{\text{surf.}} = 0 \quad (2)$$

Thus, the void-closure process can be considered as the rearrangement of atoms to reduce the surface area and GBs, thereby decreasing the energy of the entire system. Specifically, the reductions in surface area and GBs drive both void closure and grain growth.

Table 1
Potential energies per atom for intrinsic, TB, GB, and surface regions in each joint. Values in parentheses indicate the differences from the potential energy in the intrinsic region of the NT-NT joint.

Joint	Potential energies per atom (eV/atom)			
	Intrinsic	TB	GB	Surface
NC-NC	−3.443 (+0.003)	−3.434 (+0.012)	−3.368 (+0.078)	−3.003 (+0.443)
NT-NT	−3.446 (Ref.)	−3.445 (+0.001)	−3.370 (+0.076)	−2.971 (+0.475)
NC-NT	−3.445 (+0.001)	−3.442 (+0.004)	−3.369 (+0.077)	−3.000 (+0.446)

Thus far, the discussion has focused on the influence of grain structure on the energy changes of the entire system. Next, specific atoms involved in void closure and their trajectories, along with the corresponding changes in potential energy, were examined. The trajectories of specific atoms near voids at the bonding interface and their corresponding changes in potential energy are shown in Fig. 9. Fig. 9(a) and video S7 illustrate the trajectories of atoms near voids in the NC-NC joint. An atom located in the intrinsic region (atom A, at 0.0 ns) moved toward the void via the neighboring GB (at 0.5 ns) and subsequently aligned within the intrinsic region due to void closure and GB migration (from 1.0 to 10.0 ns). Similarly, an atom in the GB region (atom B, at 0.0 ns) moved along the GB toward the void (at 0.5 ns), reached the void surface (at 1.0 ns), and eventually aligned within the GB (at 5.0 ns) and the intrinsic region (at 10.0 ns). Fig. 9(b, c) present the potential energy changes of atoms A and B, respectively. For atom A (Fig. 9(b)), the potential energy temporarily increased as it transitioned from the intrinsic region to the GB region (at 0.5 ns) and then gradually stabilized. For atom B (Fig. 9(c)), the potential energy exhibited a significant increase as it moved from the GB region to the void surface (at 1.0 ns) and subsequently stabilized within the GB and intrinsic regions. In contrast, for the NT-NT joint, as shown in Fig. 9(d) and video S8, neither the atom in the intrinsic region (atom C) nor the GB region (atom D) demonstrated notable movement, even in the presence of adjacent GB migration. The changes in potential energy for atoms C and D, shown in Fig. 9(e,f), reveal that both atoms remained in consistently stable states throughout the entire simulation. These analyses indicate that atomic mobility and potential energy evolution are heavily influenced by the grain structure. Significant atomic movement and energy transitions

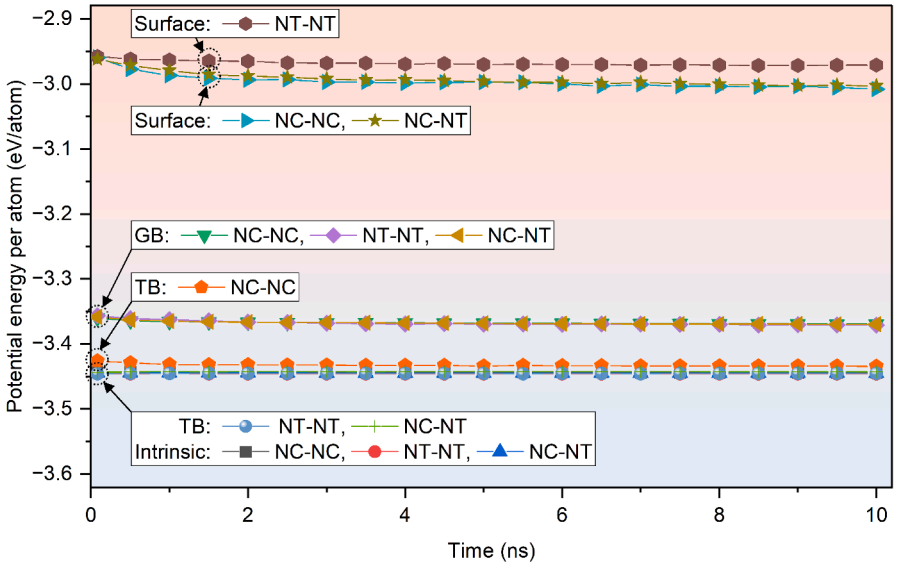

Fig. 8. Time-dependent changes in potential energy per atom in various (intrinsic, TB, GB, and surface) regions for NC-NC, NT-NT, and NC-NT joints.

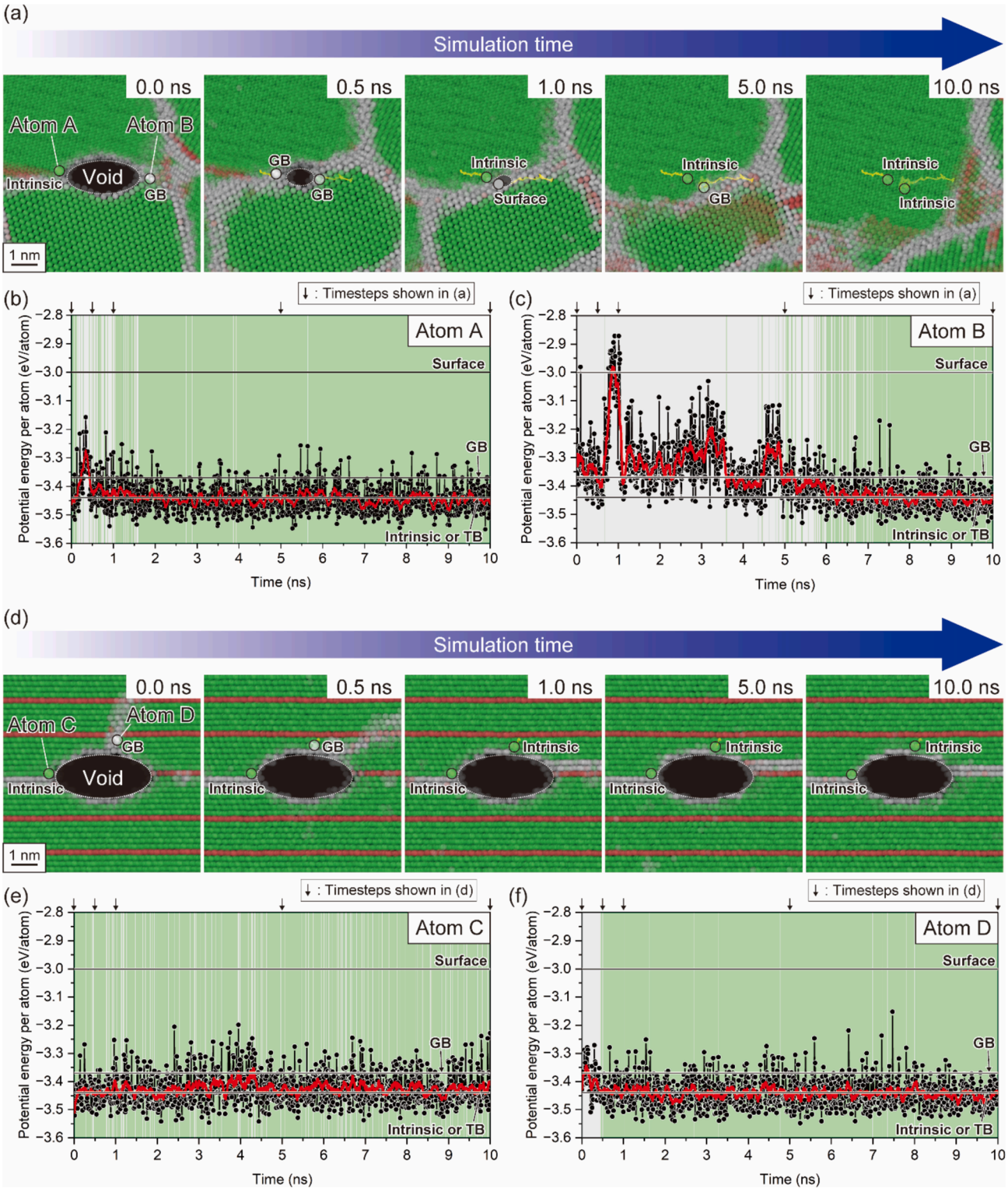

Fig. 9. Trajectories and corresponding potential energy evolution of specific atoms within intrinsic and GB structures near the bonding interface. (a) Trajectories of atoms within the intrinsic structure (atom A) and the GB structure (atom B) of the NC-NC joint. (b, c) Potential energy evolution of atom A and atom B, respectively. (d) Trajectories of atoms within the intrinsic structure (atom C) and the GB structure (atom D) of the NT-NT joint. (e, f) Potential energy evolution of atom C and atom D, respectively. In (b), (c), (e), and (f), the black plots and lines represent the raw potential energy data, while the red lines show the smoothed curve calculated using a moving average over 100 ps. The background color of the graphs indicates the structure assignment of the atoms: green for time steps associated with the intrinsic structure and gray for time steps associated with the GB, TB, or surface structure. The horizontal lines denote the potential energy per atom specific to each structure, as detailed in Table 1.

were observed in the NC-NC joint, whereas the NT-NT joint exhibited minimal displacement and consistently stable energy states.

Over the past decades, numerous studies have highlighted the significant influence of GB structures on their diffusion behaviors in FCC metals [31–36]. In general, these studies reported that a low coincidence between adjacent grains increases the GB energy and decreases the activation energy for GB diffusion. Suzuki and Mishin [32] evaluated GB diffusion across various symmetrical tilt GBs ($\Sigma = 5, 7, 9$, and 11 with tilt axes of [001], [011], and [111]) in Cu using MD simulations, finding a wide range of activation energies spanning from 0.53 to 2.13 eV. Surholt and Herzig [37] experimentally investigated the activation energies of high-angle GBs in Cu samples of different purities and reported values in the range of 0.75–0.88 eV. These activation energies for GB diffusion fall between those for lattice diffusion—2.19 eV [38]—and surface diffusion—0.38 eV on (1 0 0), 0.23–0.30 eV on (1 1 0), and 0.026 eV on (1 1 1) [39]. Furthermore, through their well-known relationship, Borisov et al. [40] showed that a low GB energy corresponds to a high activation energy for GB diffusion. These findings support the results of this study, whereby the randomly oriented NC structure displayed a slightly larger potential energy (Table 1) and significant atomic movement at its GBs (Fig. 5). In contrast, similar to the TBs in this study, the Cu {1 1 1} TB structure notably exhibited the lowest energy among [0 1 1] tilt GBs, which is almost equivalent to the intrinsic energy [41].

In addition, grain growth activates atomic movement. This process involves the reduction of the GB area through GB migration [42], whereby atoms are displaced from one grain to another. In this study, the MSD of the NC structure, which was approximately six times larger than that of the NT structure (Fig. 6), was enhanced by the GB migration processes. The mechanisms underlying GB migration have been extensively investigated [43]. Wei et al. [44] directly observed that GB migration proceeds through the cooperative shuffling of atoms across several different stable and metastable GB structures with low energies. Randomly oriented grain structures facilitate complex GB migration, which is accompanied by significant atomic movement. In contrast, unidirectional columnar grain structures are reported to undergo coarsening through the grain rotation–coalescence mechanism [45,46], resulting in minimal atomic displacement. This assumption is supported by our atomic displacement analysis (Fig. 5) and MSD (Fig. 6) results. Interestingly, the atomic movement in the NT structure was activated by combining it with the NC structure, accompanied by a decrease in the potential energy (see Fig. 5(f), Fig. 6(c)), and Fig. 7(c)). Complex GB migration accompanied by significant atomic movement may increase the possibility of atoms jumping into the void surfaces.

Based on this discussion, Fig. 10 shows schematics of the main diffusion paths and potential energy changes associated with atomic movement from the GB to the void surface in the NC and NT structures. The main void closure process can be divided into two steps: atomic movement along the GB toward the void surface (GB diffusion) and atomic movement on the void surface (surface diffusion). The corresponding diffusion coefficients (D) are expected to follow an Arrhenius-type relationship:

$$D = D_0 \exp\left(-\frac{Q}{k_b T}\right) \tag{3}$$

where D_0 is a pre-exponential factor, Q is the activation energy, k_b is the Boltzmann constant, and T is the temperature. The GB and surface diffusions contribute to the inflow of atoms into the void region and the reduction of the void curvature, respectively, resulting in a reduction in the total energy of the system. In the NC structure (Fig. 5(d) and 9(a)), the main diffusion paths were GB diffusion perpendicular to the void surface and surface diffusion parallel to the void surface. Quantitatively determining the activation energies for these diffusion paths requires a

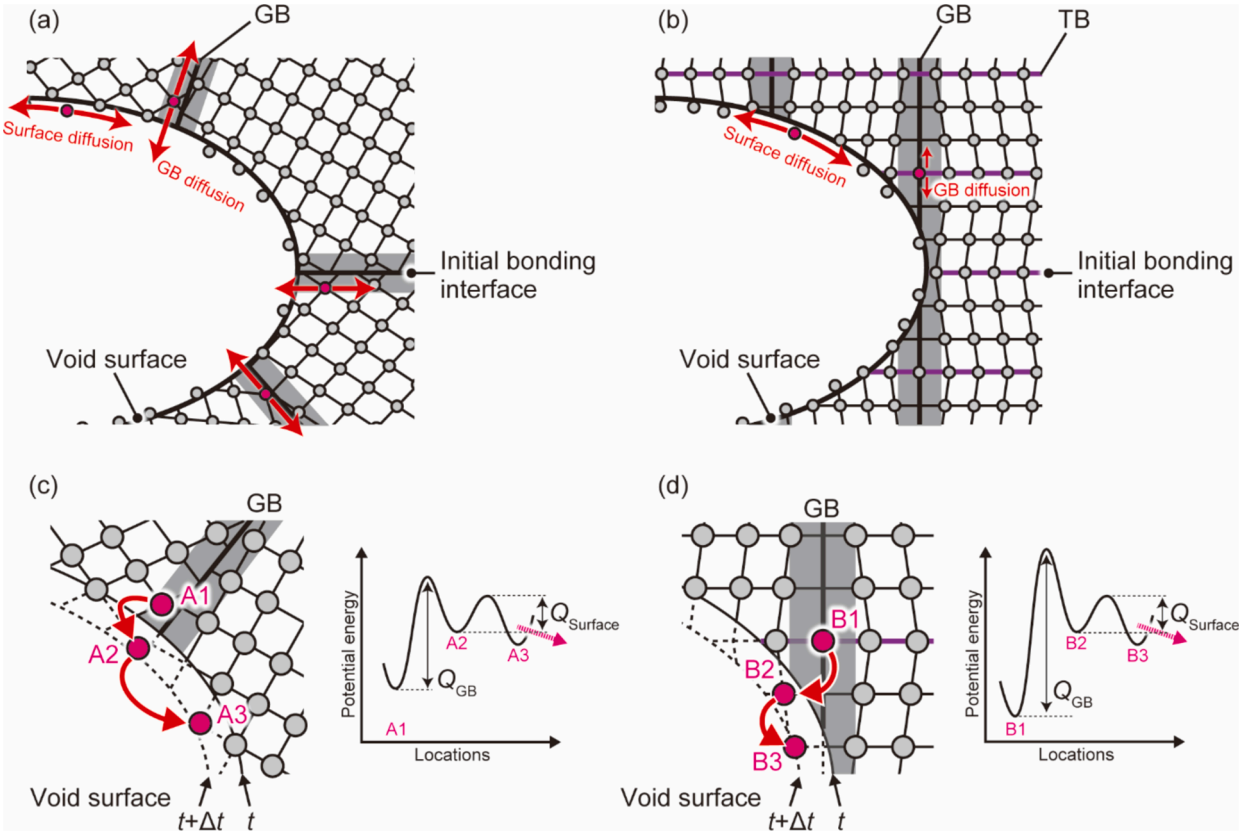

Fig. 10. Schematics of primary diffusion paths in (a) NC and (b) NT structures, and potential energy changes accompanying atomic movement from the GB to the void surface in (c) NC and (d) NT structures. Panels (c) and (d) illustrate the process of an atom moving to the void surface via GB diffusion and then to a more stable position via surface diffusion, shown as A1 → A2 → A3 (c) or B1 → B2 → B3 (d).

more detailed evaluation, which is beyond the scope of this study. However, a potential energy change is assumed, as shown in Fig. 10(c). Atoms can easily jump from a random GB (site A1, Fig. 10(c)) to the void surface (site A2, Fig. 10(c)), owing to the low activation energy of GB diffusion. GB migration during grain growth may facilitate this jump. This is followed by surface diffusion into a lower potential energy site (site A3, Fig. 10(c)). On the other hand, in the NT structure (Fig. 5(e) and 9(b)), surface diffusion is dominant, while GB diffusion is a minor process. The assumed potential energy changes (Fig. 10(d)) indicate that the high activation energy of GB diffusion inhibits atoms from jumping from the GB (site B1, Fig. 10(d)) to the void surface (site B2, Fig. 10(d)). Consequently, despite significant surface diffusion, the minimal GB diffusion does not enhance void closure.

In summary, surface diffusion contributes toward reducing void curvature, which is an important step in the void closure process. Nevertheless, GBs play an important role as they provide the primary pathway for transporting atoms to the void region. Notably, this GB-driven atomic transport mechanism is another essential step of the void closure process.

5. Conclusions

This study investigated the atomic movement behavior and void-closure mechanisms at the bonding interfaces of Cu–Cu joints with different grain structures, namely NC and NT structures. The results demonstrated that NC structures exhibited significant atomic movement at the GBs, leading to early void closure. In contrast, NT structures showed minimal atomic movement despite significant movement on the void surface, resulting in limited void closure.

Potential energy analysis revealed that NC structures experienced a significant decrease in potential energy over time, whereas NT structures maintained their quasi-stable potential energies and did not achieve void closure. These differences were attributed to the mobility of GB atoms and grain growth mechanisms, which were affected by the grain structure. The NC structure, with its random GBs, exhibited high atomic mobility due to the high potential energy and low activation energy for GB diffusion. Additionally, grain growth driven by complex GB migration further enhanced atomic mobility. In contrast, the NT structure limited the mobility of GB atoms owing to its low potential energy and high activation energy for GB diffusion, a result of its high-coincidence GB structure. Moreover, its grain growth proceeded with minimal atomic movement due to the grain rotation–coalescence mechanism, which led to a metastable state that did not promote void closure.

In conclusion, our research offers a deeper understanding of the role of grain structures in polycrystalline Cu on void-closure behavior. Randomly oriented GBs serve as the primary pathway for supplying atoms to void regions, and this GB-driven atomic transport mechanism promotes void closure. In addition, grain growth accompanied by complex GB migration activates atomic migration. Thus, polycrystalline Cu with high-density GBs shows potential for achieving low-temperature Cu–Cu bonding technology. These findings offer valuable insights for optimizing manufacturing processes and realizing low-temperature Cu–Cu bonding technology for advanced electronic interconnections. However, the instability of GB structures raises concerns regarding post-bonding stability and reliability. Balancing the trade-off between bondability and long-term stability remains a critical challenge. Further research into the material design of polycrystalline Cu utilizing GB engineering is of particular interest.

CRediT authorship contribution statement

Hiroaki Tatsumi: Writing – original draft, Visualization, Methodology, Investigation, Formal analysis, Data curation, Conceptualization. **C.R. Kao:** Writing – review & editing, Conceptualization. **Hiroshi Nishikawa:** Writing – review & editing, Supervision.

Declaration of competing interest

The authors declare that they have no known competing financial interests or personal relationships that could have appeared to influence the work reported in this paper.

Acknowledgements

This work used computational resources from the supercomputer Fugaku provided by the RIKEN Center for Computational Science through the HPCI System Research Project (Project ID: hp230440 and hp240308).

Appendix A. Supplementary data

Supplementary data to this article can be found online at https://doi.org/10.1016/j.matdes.2024.113576.

Data availability

Data will be made available on request.

References

[1] J. Kim, L. Zhu, H.M. Torun, M. Swaminathan, S.K. Lim, A PPA Study for Heterogeneous 3-D IC Options: Monolithic, Hybrid Bonding, and Microbumping, IEEE Trans. Very Large Scale Integr. VLSI Syst. 32 (2024) 401–412.
[2] C. Chen, D. Yu, K.-N. Chen, Vertical interconnects of microbumps in 3D integration, MRS Bull. 40 (2015) 257–263.
[3] C.E. Ho, S.C. Yang, C.R. Kao, Interfacial reaction issues for lead-free electronic solders, J. Mater. Sci.: Mater. Electron. 155–174 (2007).
[4] J. Li, Y. Zhang, H. Zhang, Z. Chen, C. Zhou, X. Liu, W. Zhu, The thermal cycling reliability of copper pillar solder bump in flip chip via thermal compression bonding, Microelectron. Reliab. 104 (2020) 113543.
[5] P. Zhang, S. Xue, J. Wang, New challenges of miniaturization of electronic devices: Electromigration and thermomigration in lead-free solder joints, Mater. Des. 192 (2020) 108726.
[6] Y. Qiao, H. Ma, F. Yu, N. Zhao, Quasi-in-situ observation on diffusion anisotropy dominated asymmetrical growth of Cu-Sn IMCs under temperature gradient, Acta Mater. 217 (2021) 117168.
[7] J.H. Lau, Recent Advances and Trends in Cu–Cu Hybrid Bonding, IEEE Trans. Compon. Packaging Manuf. Technol. 13 (2023) 399–425.
[8] Y.-G. Lee, M. McInerney, Y.-C. Joo, I.-S. Choi, S.E. Kim, Copper Bonding Technology in Heterogeneous Integration, Electron. Mater. Lett. 20 (2024) 1–25.
[9] T.-H. Hung, Y.-M. Pan, K.-N. Chen, Stress issue of vertical connections in 3D integration for high-bandwidth memory applications, Memories - Materials, Devices, Circuits and Systems 4 (2023) 100024.
[10] Y. Ikegami, T. Onodera, M. Chiyozono, A. Sakamoto, K. Shimizu, Y. Kagawa, H. Iwamoto, Study of ultra-fine 0.4 μm pitch wafer-to-wafer hybrid bonding and impact of bonding misalignment, in: 2024 IEEE 74th Electronic Components and Technology Conference (ECTC), IEEE, 2024: pp. 299–304.
[11] S. Jangam, S.S. Iyer, Silicon-Interconnect Fabric for Fine-Pitch (≤10 μm) Heterogeneous Integration, IEEE Trans. Compon. Packaging Manuf. Technol. 11 (2021) 727–738.
[12] H. Park, H. Seo, Y. Kim, S. Park, S.E. Kim, Low-Temperature (260° C) Solderless Cu–Cu Bonding for Fine-Pitch 3-D Packaging and Heterogeneous Integration, IEEE Trans. Compon. Packaging Manuf. Technol. 11 (2021) 565–572.
[13] S.-C. Yang, J.-J. Ong, C. Chen, Effect of bonding interfacial microstructures on the properties and reliabilities of Cu–Cu joints, J. Mater. Res. Technol. 32 (2024) 3490–3499.
[14] C.-M. Liu, H.-W. Lin, Y.-C. Chu, C. Chen, D.-R. Lyu, K.-N. Chen, K.N. Tu, Low-temperature direct copper-to-copper bonding enabled by creep on highly (111)-oriented Cu surfaces, Scr. Mater. 78–79 (2014) 65–68.
[15] C.-M. Liu, H.-W. Lin, Y.-S. Huang, Y.-C. Chu, C. Chen, D.-R. Lyu, K.-N. Chen, K.-N. Tu, Low-temperature direct copper-to-copper bonding enabled by creep on (111) surfaces of nanotwinned Cu, Sci. Rep. 5 (2015) 9734.
[16] B. Rebhan, K. Hingerl, Physical mechanisms of copper-copper wafer bonding, J. Appl. Phys. 118 (2015) 135301.
[17] Y. Wang, Y.T. Huang, Y.X. Liu, S.P. Feng, M.X. Huang, Thermal instability of nanocrystalline Cu enables Cu-Cu direct bonding in interconnects at low temperature, Scr. Mater. (2022). https://www.sciencedirect.com/science/article/pii/S1359646222003967.
[18] C. He, J. Zhou, R. Zhou, C. Chen, S. Jing, K. Mu, Y.-T. Huang, C.-C. Chung, S.-J. Cherng, Y. Lu, K.-N. Tu, S.-P. Feng, Nanocrystalline copper for direct copper-to-copper bonding with improved cross-interface formation at low thermal budget, Nat. Commun. 15 (2024) 7095.
[19] C. Li, D. Li, X. Tao, H. Chen, Y. Ouyang, Molecular dynamics simulation of diffusion bonding of Al–Cu interface, Modell. Simul. Mater. Sci. Eng. 22 (2014) 065013.

[20] A. Xydou, S. Parviainen, M. Aicheler, F. Djurabekova, Thermal stability of interface voids in Cu grain boundaries with molecular dynamic simulations, J. Phys. D Appl. Phys. 49 (2016) 355303.
[21] C.-D. Wu, C.-F. Liao, Molecular dynamics simulation of the direct bonding of (111)-oriented nanotwinned Cu and its related mechanical behavior, J. Phys. Chem. Solids 187 (2024) 111872.
[22] H. Tatsumi, C.R. Kao, H. Nishikawa, Impact of crystalline orientation on Cu–Cu solid-state bonding behavior by molecular dynamics simulations, Sci. Rep. 13 (2023) 1–10.
[23] H.-Y. Hsiao, C.-M. Liu, H.-W. Lin, T.-C. Liu, C.-L. Lu, Y.-S. Huang, C. Chen, K.N. Tu, Unidirectional growth of microbumps on (111)-oriented and nanotwinned copper, Science 336 (2012) 1007–1010.
[24] X. Zhao, C. Lu, A.K. Tieu, L. Pei, L. Zhang, L. Su, L. Zhan, Deformation mechanisms in nanotwinned copper by molecular dynamics simulation, Mater. Sci. Eng. A 687 (2017) 343–351.
[25] P. Hirel, Atomsk: A tool for manipulating and converting atomic data files, Comput. Phys. Commun. 197 (2015) 212–219.
[26] A.P. Thompson, H.M. Aktulga, R. Berger, D.S. Bolintineanu, W.M. Brown, P.S. Crozier, P.J. in 't Veld, A. Kohlmeyer, S.G. Moore, T.D. Nguyen, R. Shan, M.J. Stevens, J. Tranchida, C. Trott, S.J. Plimpton, LAMMPS - a flexible simulation tool for particle-based materials modeling at the atomic, meso, and continuum scales, Comput. Phys. Commun. 271 (2022) 108171.
[27] Y. Mishin, M.J. Mehl, D.A. Papaconstantopoulos, A.F. Voter, J.D. Kress, Structural stability and lattice defects in copper: Ab initio, tight-binding, and embedded-atom calculations, Phys. Rev. B Condens. Matter 63 (2001) 224106.
[28] A. Stukowski, Visualization and analysis of atomistic simulation data with OVITO–the Open Visualization Tool, Modell. Simul. Mater. Sci. Eng. 18 (2009) 015012.
[29] P.M. Larsen, S. Schmidt, J. Schiøtz, Robust structural identification via polyhedral template matching, Modell. Simul. Mater. Sci. Eng. 24 (2016) 055007.
[30] A. Stukowski, Computational Analysis Methods in Atomistic Modeling of Crystals, JOM 66 (2014) 399–407.
[31] P. Keblinski, D. Wolf, S.R. Phillpot, H. Gleiter, Self-diffusion in high-angle fcc metal grain boundaries by molecular dynamics simulation, Philos. Mag. A 79 (1999) 2735–2761.
[32] A. Suzuki, Y. Mishin, Atomistic modeling of point defects and diffusion in copper grain boundaries, Interface Sci. 11 (2003) 131–148.
[33] B. Schönfelder, G. Gottstein, L.S. Shvindlerman, Comparative study of grain-boundary migration and grain-boundary self-diffusion of [001] twist-grain boundaries in copper by atomistic simulations, Acta Mater. 53 (2005) 1597–1609.
[34] M.I. Mendelev, H. Zhang, D.J. Srolovitz, Grain boundary self-diffusion in Ni: Effect of boundary inclination, J. Mater. Res. 20 (2005) 1146–1153.
[35] D. Turnbull, R.E. Hoffman, The effect of relative crystal and boundary orientations on grain boundary diffusion rates, Acta Metall. 2 (1954) 419–426.
[36] P. Schweizer, A. Sharma, L. Pethö, E. Huszar, L.M. Vogl, J. Michler, X. Maeder, Atomic scale volume and grain boundary diffusion elucidated by in situ STEM, Nat. Commun. 14 (2023) 7601.
[37] T. Surholt, C. Herzig, Grain boundary self-diffusion in Cu polycrystals of different purity, Acta Mater. 45 (1997) 3817–3823.
[38] S.M. Klotsman, Y.A. Rabovskiy, V.K. Talinskiy, A.N. Timofeyev, Volume Diffusion of Gallium-67 and Germanium-68 in Copper, Phys. Met. Metall. 31 (1971) 214–216.
[39] C.L. Liu, J.M. Cohen, J.B. Adams, A.F. Voter, EAM study of surface self-diffusion of single adatoms of fcc metals Ni, Cu, Al, Ag, Au, Pd, and Pt, Surf. Sci. (1991). https://www.sciencedirect.com/science/article/pii/003960289190604Q.
[40] V.T. Borisov, V.M. Golikov, G.V. Scherbedinskiy, Relation between diffusion coefficients and grain boundary energy, Phys. Met. Metall 17 (1964) 881–885.
[41] U. Wolf, F. Ernst, T. Muschik, M.W. Finnis, H.F. Fischmeister, The influence of grain boundary inclination on the structure and energy of $\sigma = 3$ grain boundaries in copper, Philos. Mag. A 66 (1992) 991–1016.
[42] J.E. Burke, D. Turnbull, Recrystallization and grain growth, Prog. Phys. Met. / Uspehi Fiziki Metallov 3 (1952) 220–292.
[43] G.S. Rohrer, I. Chesser, A.R. Krause, S. Kiana Naghibzadeh, Z. Xu, K. Dayal, E. A. Holm, Grain Boundary Migration in Polycrystals, Annu. Rev. Mater. Res. 53 (2023) 347–369.
[44] J. Wei, B. Feng, R. Ishikawa, T. Yokoi, K. Matsunaga, N. Shibata, Y. Ikuhara, Direct imaging of atomistic grain boundary migration, Nat. Mater. 20 (2021) 951–955.
[45] A.J. Haslam, S.R. Phillpot, D. Wolf, D. Moldovan, H. Gleiter, Mechanisms of grain growth in nanocrystalline fcc metals by molecular-dynamics simulation, Mater. Sci. Eng. A 318 (2001) 293–312.
[46] D. Moldovan, D. Wolf, S.R. Phillpot, A.J. Haslam, Role of grain rotation during grain growth in a columnar microstructure by mesoscale simulation, Acta Mater. 50 (2002) 3397–3414.